Graphene-Paper-Based Electrodes on Plastic and Textile Supports as New Platforms for Amperometric Biosensing

(article starts on next page)

Graphene-Paper-Based Electrodes on Plastic and Textile Supports as New Platforms for Amperometric Biosensing

Fabrizio Poletti, Alessandra Scidà, Barbara Zanfrognini, Alessandro Kovtun, Vitaliy Parkula, Laura Favaretto, Manuela Melucci, Vincenzo Palermo,* Emanuele Treossi,* and Chiara Zanardi*

The possibility of exfoliating graphite into graphene sheets allows the researchers to produce a material, termed "graphene paper" (G-paper), conductive as graphite but more flexible and processable. G-paper is already used for electronic applications, like conductors, antennas, and heaters, outperforming metal conductors thanks to its high flexibility, lightness, chemical stability, and compatibility with polymeric substrates. Here, the effectiveness in the use of G-paper for the realization of electrodes on flexible plastic substrates and textiles, and their applicability as amperometric sensors are demonstrated. The performance of these devices is compared with commercial platforms made of carbon-based inks, finding that they outperform commercial devices in sensing nicotinamide adenine dinucleotide (NADH), a key molecule for enzymatic biosensing; the electrodes can achieve state-of-the-art sensitivity ($107.2\ \mu A\ mM^{-1}\ cm^{-2}$) and limit of detection ($0.6 \times 10^{-6}\ M$) with no need of additional functionalization. Thanks to this property, the stable deposition of a suitable enzyme, namely lactate dehydrogenase, on the electrode surface is used as a proof of concept of the applicability of this new platform for the realization of a biosensor. The possibility of having a single material suitable for antennas, electronics, and now sensing opens new opportunities for smart fabrics in wearable electronic applications.

F. Poletti, C. Zanardi
Department of Chemical and Geological Sciences
University of Modena and Reggio Emilia
Modena 41125, Italy
E-mail: chiara.zanardi@unimore.it
A. Scidà, B. Zanfrognini, A. Kovtun, V. Parkula, L. Favaretto, M. Melucci,
V. Palermo, E. Treossi, C. Zanardi
Institute for the Organic Synthesis and Photoreactivity
National Research Council
Bologna 40129, Italy
E-mail: vincenzo.palermo@isof.cnr.it; emanuele.treossi@isof.cnr.it
V. Palermo
Department of Industrial and Materials Science
Chalmers University of Technology
Gothenburg S-41296, Sweden

1. Introduction

Disposable electrochemical platforms are widely employed in scientific research as well as in practical applications, since they allow a simple, fast, low-cost, and reproducible analyte detection using low amounts of solution. Nowadays, to suit a wide range of applications, there are several disposable devices available on the market, possessing different geometries, made on flexible or solid supports, and typically built with conventional conducting materials (e.g., carbon-based inks or Au thin films). They are generally produced on industrial scale by inkjet, gravure, and screen printing. These techniques allow the realization of devices possessing best performance in terms of resolution, reproducibility, low production costs and time, flexible manufacturing, and low amount of waste generated.[1,2] This notwithstanding, there is the growing interest in innovative printing techniques, e.g., 3D printing,[3] laser ablation,[4] and the use of cutting printers.[5]

Disposable platforms present on the market are commonly obtained using conventional graphite-based inks;[6,7] the resulting devices possess the right conductivity for the use in the electrochemical field. However, their analytical performance in the detection of several species of industrial and clinical interest (e.g., urea, glucose, lactate, dopamine, ascorbic acid, uric acid, and H_2O_2) is often very scarce, since high overpotentials normally affect charge-transfer processes at these electrochemical platforms, thus limiting the sensitivity and selectivity of the detection, and by-products of electrochemical reactions passivate the electrode surface, thus affecting the repeatability of the sensor response.[8,9] To overcome these drawbacks, the surface of the working electrode is generally modified by different coating materials, e.g., conducting polymers, metal or carbon nanomaterials, or redox active metal complexes.[8] They are mainly responsible for the activation of electrocatalytic processes, i.e., a decrease of the potential values required to achieve oxidation or reduction of the target analyte with respect to conventional electrode surfaces; this effect increases the selectivity of the sensor when applied in analyses of complex real matrices, since the number of species that can be oxidized or reduced at the same potential values decreases, and

the sensitivity of the sensor response increases since voltametric peaks result sharper; film coatings modifying the electrode surface could also induce antifouling properties, thus improving the stability of the sensor response.

Deposition of these coatings is generally performed by drop-casting, spin-coating, or electrodeposition methods;[9,10] approaches based on a preliminary electrochemical reduction[11] or oxidation[12] of the surface to modify the number of functional groups present[13] were also proposed. However, the deposition of a coating in a step following the sensor fabrication increases the production costs, and may decrease the stability, i.e., repeatability, and the reproducibility of the sensor response due to a poor mechanical stability.

An alternative, less exploited, route to easily produce effective electrochemical sensors implies a preliminary modification of the printing inks by the addition of selected nanomaterials or redox mediators.[7] A few examples from the literature are the addition of MnO_2 to detect coenzyme Q10 and α-lipoic acid, simultaneously;[14] of Prussian blue (PB) to detect H_2O_2 produced by an enzymatic reaction,[15] of ferrocene to detect Cd(II), Cu(II), and Pb(II);[16] and carbon black for the analysis of phenol derivatives and H_2O_2.[17] However, only a low amount of the active element can be added, since the ink should possess specific viscosity and surface tension, fitting a narrow window of allowed variability, which depends on the printer employed. In addition, solvents, viscosity modifiers, and surfactants, which should be added to assure the required stability of the ink, may negatively impact the performance of the resulting sensor, especially considering nonvolatile additives, which remain on the substrate after the deposition, and cannot be removed by washing.[1] To overcome these drawbacks and achieve good and reproducible results, a possible solution could be the development of a sensor entirely fabricated with the active element, thus simplifying the productive process, and increasing the stability and the analytical response of the sensor.

In recent years, graphene and its related materials (GRM) have attracted a growing interest in the scientific community, thanks to remarkable structural and electronic properties, and to the actual use of very simple and scalable synthetic methods.[18] GRM now find application in various technological fields, thus receiving attention also from industrial research.[19] They are increasingly exploited in electrochemical (bio)sensing thanks to their nanosized dimensions, which allow a great number of oxidized residues on the surface to be well exposed to the surrounding environment; specific oxygen-containing moieties are responsible for the activation of electrocatalytic processes toward several species[20–23] or they can be exploited to act as binding sites of (bio)molecules.[24–26] Thanks to these properties, inks based on GRM were also developed.[27,28]

All GRM have different amounts and types of moieties on the surface, depending on the starting material and on the procedure employed for their synthesis;[29,30] it is important to know which moieties are present, in order to use the most suited material for each application. Typically, in electrochemical (bio)sensing applications, reduced graphene oxide (rGO) is preferred to pristine graphene, as it contains a significant number of oxidized functional groups to activate effective electrocatalytic processes; it is soluble in water; and it can be easily functionalized by defined (bio)molecules. However, pristine graphene possesses higher conductivity, which makes it easier

to be employed without any preliminary reduction. Trying to combine the advantages of both these materials, we focused our attention on graphene paper (G-paper), a particular GRM featuring planar shape and good processability, only seldom employed in electroanalysis. Depending on the specific GRM used for the preparation (e.g., reduced graphene oxide or graphite nanoplatelets) or on the production technique adopted (e.g., vacuum filtration, spray coating, or electrophoretic deposition),[31–33] this material can have good mechanical and electrical properties, excellent chemical stability and, according to our previous work, can withstand more than 10 000 bending cycles without variation of its electrical conductivity.[34] It is also highly versatile, and various functional guest nanomaterials can be included, namely metals, semiconductors, and polymers, allowing G-paper to be employed in numerous applications. In particular, self-standing G-paper was studied for the development of Li-ion batteries and supercapacitors,[35] flexible electronics,[34] heat transfer materials,[33] also by improving its electrical properties with the inclusion of TiO_2,[36] Co_3O_4,[37] MnO_2,[38,39] carbon nanotubes and NiS,[40] polyaniline,[41–44] and VO_2.[45] Other explored applications of G-paper are electrodes for dye-sensitized solar cells[46–48] and gas barriers,[49] after modification with polyethyleneimine as well.[50,51]

G-paper was also studied for the development of amperometric sensors, but only acting as a free-standing support for redox mediators or nanoparticles (NPs). Some examples include the addition of Prussian blue nanoparticles to detect glucose and H_2O_2,[52] Pt nanoparticles,[53] and MnO_2 nanowires[54] to detect H_2O_2, and of Ag nanoparticles and of poly(methylene blue) (PMB) for nicotinamide adenine dinucleotide (NADH) oxidation.[55] There are also a couple of examples of sensors, where G-paper is used without any modification to detect urea;[56,57] however, in these cases, the material is employed as a coating of commercial electrodes, with the drawbacks being previously listed. Studies concerning the electrocatalytic properties of this material toward analytes of biological interest were only performed on graphite nanoplatelets deposited on a bulk carbon electrode.[58]

In this work, we discuss the performance of a newly developed three-electrode cell made of commercial G-paper prepared from graphite nanoplatelets,[34] fixed on a flexible plastic support, namely poly(ethylene terephthalate) (PET), Kapton, or cotton textiles (**Figure 1**). We demonstrate that our G-paper electrode platforms (GPPs) can be successfully employed as an electrochemical sensor in smart fabrics without any further modification of the surface; tests with redox active species undergoing a reversible charge-transfer, namely 1,1′-ferrocenedimethanol (Fc), electrochemical impedance spectroscopy (EIS), and four-point probe (FPP) resistivity measurements showed that the material possesses suitable conductivity for the use in the electrochemical frame. Tests with NADH, a co-factor for many dehydrogenase-type enzymes, indicated that the material features suitable electrocatalytic properties for the realization of effective biosensors, resulting in a sensitivity of $107.2\,\mu A\,mM^{-1}\,cm^{-2}$ and a limit of detection (LOD) of 0.6×10^{-6} M; this can be ascribable to oxidized moieties naturally present on the surface of GRMs.[21] The unprecedented electroanalytical performance of this novel electrochemical device was compared with that of two commercial screen-printed electrodes (SPEs) with a similar cell geometry, made of a carbon-based ink (C-SPE) and of a graphite-based ink (Gr-SPE), respectively; we should
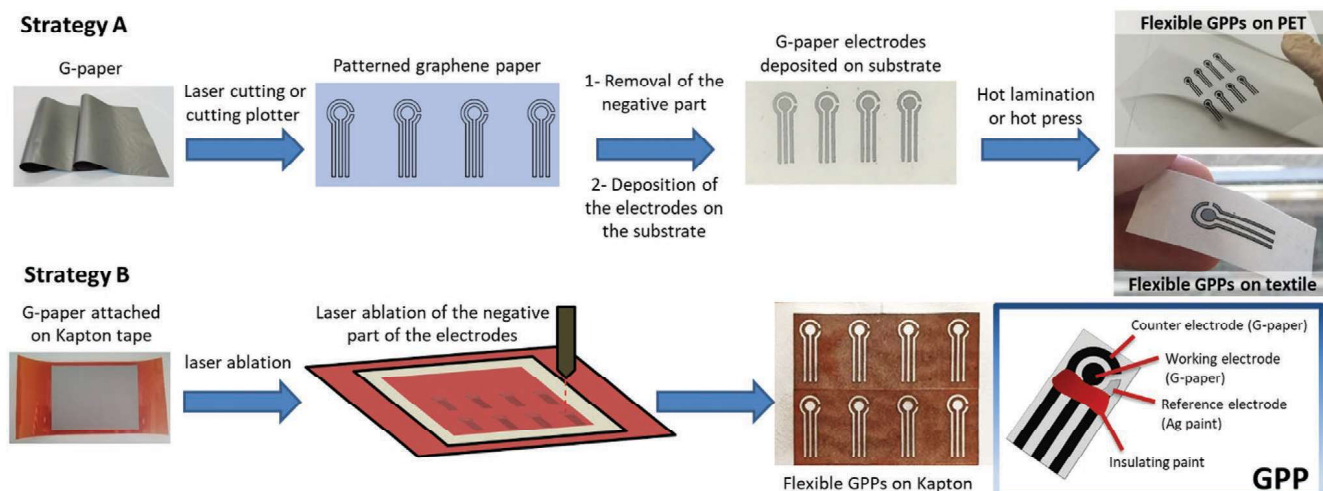
Figure 1. Two different strategies used for the preparation of flexible GPPs on plastic substrates and on textile: strategy (A) by cutting and strategy (B) by laser ablation. The scheme of the resulting three-electrode platform is reported in the right bottom box.

remark that inks for screen printing are not entirely composed of conductive carbon, but they also contain a significant fraction of binders and other additives to allow processability.[2,59] Finally, an enzyme, namely lactate dehydrogenase (LDH), was anchored to prove the applicability of the electrochemical platform in biosensing, with an enzyme requiring the use of NADH as the co-factor. The technological advances shown in this work, also considering the well-established uses of G-paper, open new possibilities for wearable electronic applications.
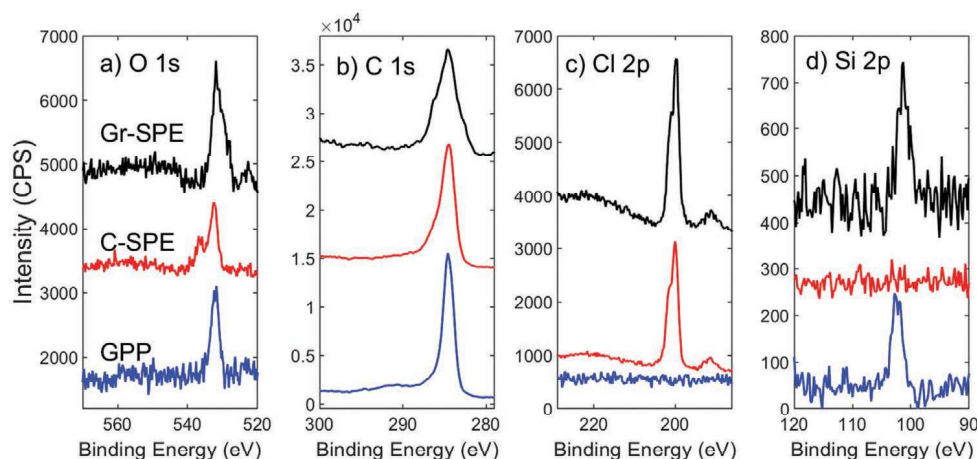
2. Results and Discussion

2.1. Spectroscopic Characterization of GPP Surface

GPPs were fabricated starting from commercial G-paper (obtained from Nanesa), as detailed in the "Experimental Section" and schematized in Figure 1.

The composition of the surface was defined by X-ray photoelectron spectroscopy (XPS). Figure S1 (Supporting Information) reports the whole XPS spectrum acquired, whereas **Figure 2** considers the single contributions ascribable to the atoms present on the surface. They show that GPP is composed of carbon (96 at%), oxygen (2 at%), and silicon (<2 at%), in strict analogy with pristine G-paper (Table S1, Supporting Information), thus confirming that the fabrication processes of the electrochemical platform did not affect the composition of the material. No metallic contaminations were observed within the XPS sensitivity range.

We observed some traces of silicon in the oxidized form ($R\!-\!SiO_2$ or $R\!-\!SiO\!-\!R$), evidenced by the Si 2p peak at 102.4 eV,[60] suggesting the use of silicon-based supports for the manufacture or the packaging of G-paper. Si, in fact, is only present in the external surface of the sample, as concluded by considering analogous XPS spectra recorded on G-paper after the mechanical peeling of the surface with scotch tape, which resulted completely free from any contribution ascribable to Si (Table S1, Supporting Information). However, traces of Si do not affect the electrochemical performance of the GPP (see hereafter), so that the material can be used without any pretreatment.

Figure 2. XPS spectra of Gr-SPE (black), C-SPE (red), and GPP (blue): a) O 1s, b) C 1s, c) Cl 2p, and d) Si 2p signals.

ADVANCED
SCIENCE NEWS
www.advancedsciencenews.com

ADVANCED
FUNCTIONAL
MATERIALS
www.afm-journal.de

The fitting of the C 1s peak[61] after peeling revealed that ≈97 at% of carbon is in the aromatic form (C—C sp^2, 284.4 eV), while the sum of residual defects, as aliphatic carbon (C—C sp^3, 285.0 eV), hydroxyl (C—OH, 285.7 eV), epoxy (C—O—C, 286.7 eV), carbonyl (C=O, 288.0 eV), and carboxyl (O—C=O, 289.1 eV) was ≈3 at% (Figure S2 and Table S2, Supporting Information). Although the exact composition of G-paper is proprietary and undisclosed by the producer, XPS results did not show the presence of other additives or binders, indicating that the material totally consists of graphite nanoplatelets.

Similar fitting was also performed for two commercial SPEs possessing similar geometry and chemical composition, since screen-printed platforms are the most widely exploited disposable electrochemical platforms; they consisted of C-SPE (obtained from Metrohm-Dropsens) and Gr-SPE (Sense4Med) (see the "Experimental Section" for details). In both cases, XPS spectra showed the presence of Cl and Si bonded to C, probably due to some component used as binder to allow processability of the ink for screen printing, as shown in our previous work.[21] These contributions did not allow us to assign specific peaks to the sp^3 components; thus, the only reliable result of the fit in these cases was the estimation of the sp^2 fraction, which is univocally assigned by the asymmetric peak at 284.4 eV. We could observe that C-SPE and Gr-SPE surfaces possess a significantly lower fraction of aromatic carbon, 82.3 ± 0.8 and 60 ± 3 at%, respectively. Furthermore, the amount of oxygen is significantly larger (4.4 at% in C-SPE and 10 at% in Gr-SPE) while, as stated before, they both contain a considerable amount of Cl.

2.2. Electrochemical Behavior of GPP

Preliminary electrochemical tests in the absence and presence of a reversible redox probe, namely Fc, were performed to understand if the newly developed GPPs can be effectively used as an electrochemical platform for the realization of amperometric sensors; the first set of tests was performed on electrochemical platforms realized on PET, being the most similar substrate to devices actually present on the market. A repeatable response, not affected by Ohmic resistance, was obtained from cyclic voltammetry (CV) responses recorded in the pure electrolyte solution (**Figure 3**a, dashed line). GPPs showed a fairly high background current mainly ascribable to a capacitive component. It is even higher than that typical of similar systems; current measured with GPP was ≈200% that of a commercial C-SPE coated with graphene[62] and 500% that of a C-SPE electrode coated with electrochemically reduced GO.[21]

We could have a better understanding of the electrochemical behavior of GPPs by testing their resistance to charge transfer with respect to a species undergoing a reversible oxidation process, namely Fc. The CV response (Figure 3a, solid line) showed the typical shape of a reversible Faradic process controlled by diffusion. A difference between oxidation and reduction potentials of 80 mV, a linear correlation between the intensity of the oxidation peak and the square root of the potential scan rate (Figure S3, Supporting Information) according to the Randles–Sevcik equation, and a ratio between the anodic and the cathodic peak heights close to 1. These results indicated that GPP behaves similarly to conventional metal- or carbon-based electrodes normally used as sensor platforms; thus, it is suitable to be used as an electrochemical device. This is in agreement with XPS analysis of the starting G-paper, which showed a material mostly composed of a sp^2 hybridized carbon and a low amount of oxidized moieties. According to a previous work,[21] in fact, a low amount of oxygen-containing groups guarantees the high conductivity of the material without any preliminary reduction.

Sheet resistance of the working electrode of GPP was compared to those of commercial C-SPE and Gr-SPE by FPP measurements (Figure S6, Supporting Information), resulting 0.095 ± 0.025, 20 ± 10, and 50 ± 10 Ω sq^{-1}, respectively. The different behaviors of the three-electrode platforms were confirmed by EIS measurements, performed at open-circuit potential (+0.20 V for all electrode surfaces) in a 1:1 molar ratio
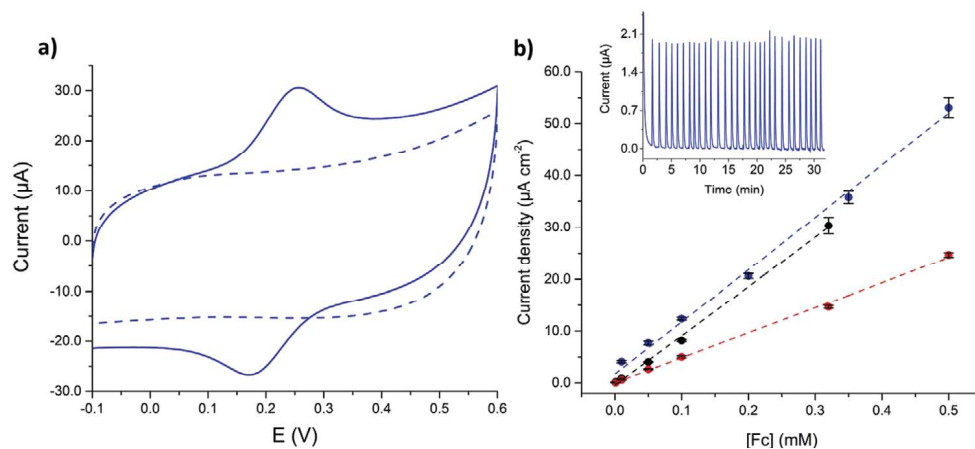
Figure 3. a) CV scans recorded at GPP on PET in 0.1 M LiClO$_4$ and 0.1 M KCl, in the absence (dashed line) and in the presence (solid line) of 0.5×10^{-3} M Fc, 0.05 V s^{-1} potential scan rate. b) Calibration plot obtained for analysis of Fc in 0.1 M LiClO$_4$ and 0.1 M KCl in FIA (1.0 mL min^{-1}, $E = +0.30$ V) at six concentration levels on GPP on PET (blue symbols), C-SPE (red symbols), and Gr-SPE (black symbols). Dashed lines show the fitting obtained by the least squares method (in all cases $R^2 > 0.99$); each solution was injected at least ten times and the standard deviation is reported in the calibration. An exemplificative FIA response at +0.30 V for 30 consecutive injections of 0.1×10^{-3} M Fc at a GPP is reported in the inset.

**ADVANCED
SCIENCE NEWS**

www.advancedsciencenews.com

**ADVANCED
FUNCTIONAL
MATERIALS**

www.afm-journal.de

$[Fe(CN)_6]^{3-/4-}$ solution in the 0.05–10 000 Hz frequency range. In all cases, the Nyquist plots (Figure S7, Supporting Information) in the high-frequency region evidenced the typical semicircle, whose diameter gave us a measure of the charge-transfer resistance (R_{ct}) of the material. Fitted values resulted in 0.27 ± 0.05, 1.58 ± 0.02, and 49.7 ± 5.0 kΩ for GPP, C-SPE, and Gr-SPE, respectively.

The occurrence of a reversible charge transfer involving Fc oxidation at all the electrode surfaces allows us to calculate the electroactive surface, according to the Randles–Sevcik equation. In the case of GPP, the active surface resulted 2.6 times higher than the mere geometric area of the working electrode, while both Gr-SPE and C-SPE show a ratio of ≈0.7, probably due to the presence of insulating agents added to the ink formulations to make the material printable and to achieve mechanical stability of the electrodes. To better understand the origin of the high electroactive surface observed for GPP, we measured the adsorption isotherm of N_2 at G-paper and performed Brunauer–Emmett–Teller (BET) analysis. This allowed us to estimate a specific surface area (SSA) of 15 m^2 g^{-1} due to the presence of pores with a dimension ranging between 2 and 50 nm, except some with a dimension of 100 nm (see Section S4 in the Supporting Information). The obtained SSA of GPP has the same order of magnitude as graphite nanoplatelets employed in the production of G-paper (25–30 m^2 g^{-1}),[63] and we could also calculate that the area of the working electrode exposed to the N_2 atmosphere is >800 times higher than the mere geometric area. This is, obviously, an overestimation of the actual electroactive surface, but indicates that the high values of both capacitive current and electroactive surface could find a physical explanation in the mesoporous structure of G-paper.

A further confirmation of the rough surface of G-paper was obtained from scanning electron microscopy (SEM) images (**Figure 4**). The surface resulted very wrinkled and, most notably, the different graphene foils composing the material were still well evident; they can contribute to increase the electroactive area of the working electrode, when exposed to the solution. Even after the fabrication process of GPP, G-paper retains the same morphology (Figure S10, Supporting Informa-
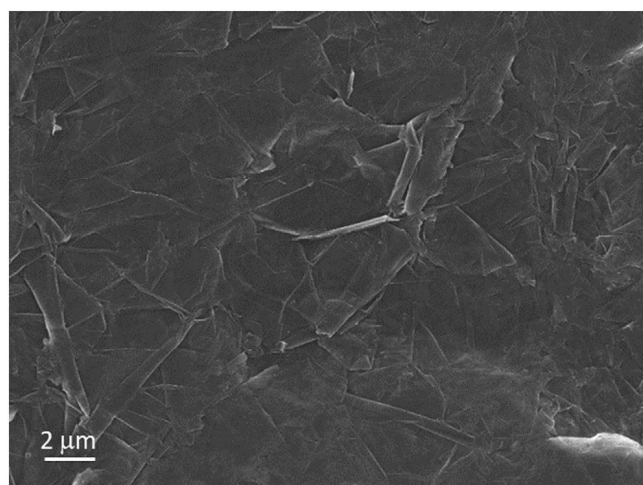
Figure 4. SEM image collected on the surface of G-paper.

tion), which is quite different from that of Gr-SPE and C-SPE (Figure S11, Supporting Information).

Therefore, G-paper has a chemical purity and an excellent surface quality, comparable to bulk graphite, but with a mesoporous structure and sheets not perfectly stacked or even partially folded. The large graphene foils composing the nanostructure of GPP and the high fraction of carbon in aromatic form are the main elements, which can contribute to the high electroactive surface observed. On the contrary, C-SPE and Gr-SPE present a high amount of a chlorine-based polymeric binder that partially hinders the conductivity of the carbon-based ink; the fraction of the insulating binder present in these formulation can be roughly estimated from XPS results and on considering polyvinyl chloride structure ($-C_2H_3Cl-$), i.e., a species with a Cl:C ratio of 1:2, as a possible component. It resulted about 24% of geometrical surface in C-SPE and 41% in Gr-SPE.

While most of electrochemical tests are performed in batch, stationary conditions, we decided to test the analytical performance of GPPs in a flow system, to check the suitability of the device for on-line measurements, e.g., for the real-time monitoring of biomarkers in a complex matrix.[64] In this case, a potentiostatic technique was adopted after inserting the device in an instrumental configuration typical of flow injection analysis (FIA). Preliminary tests were once more obtained with injections of Fc, as a benchmark species undergoing an ideal charge-transfer process; 30 consecutive injections of 0.1×10^{-3} M Fc solution (Figure 3b, inset) demonstrated that the obtained responses were highly repeatable, as testified by the value of relative standard deviation (RSD), resulting in 3.1%. In addition, the baseline was stable for a considerable amount of time (over 30 min), highlighting the possibility of using GPP to detect analytes online, i.e., in a continuous flow of sampling solution. This analysis was repeated for five more concentration levels, ranging from 1×10^{-6} to 0.50×10^{-3} M, obtaining a linear correlation between the peak current and the concentration of Fc (Figure 3b), with a sensitivity of (100.6 ± 2.1) µA mM^{-1} cm^{-2}. The electrochemical performance of GPP was compared with that of commercial C-SPE and Gr-SPE devices, whose sensitivity values to Fc at the same potential were (48.4 ± 0.7) and (95.1 ± 3.3) µA mM^{-1} cm^{-2}, respectively, indicating that the sensitivity in the detection of redox active species is comparable, or even superior, to that of commercial electrode platforms. The performance of GPP for Fc oxidation (see Table S3 in the Supporting Information) suggests that this new electrode platform can be successfully adopted for the determination of species of analytical interest even in a flow system. In particular, the sensitivity and the precision of the calibration (measured as the standard deviation of the calibration, $s_{y,x}$) are high irrespective of the background currents previously observed in the absence of redox active species, normally constituting a source of fluctuation of the amperometric signal. The negligible effect of the background currents obtained at GPP was also confirmed by the LOD, calculated as three times the standard deviation of the blank signal. It resulted well comparable to that of commercial electrochemical platforms tested under the same experimental conditions.

Quite interestingly, GPPs can also be employed in pulsed electrochemical techniques, since Fc led us to record

**ADVANCED
SCIENCE NEWS**
www.advancedsciencenews.com

**ADVANCED
FUNCTIONAL
MATERIALS**
www.afm-journal.de

well-resolved voltammetric traces also in differential pulse voltammetry (DPV) (Figure S5 and Table S4, Supporting Information), thus increasing the possible applications of these electrodes in the sensor frame, toward analytical detections requiring a voltammetric approach.

These results were repeated on GPPs realized on both cotton and Kapton supports, demonstrating that the underlying material does not affect the properties of the active electrodes (see Figure S4 in the Supporting Information) and that G-paper-based devices can be used as platforms for the realization of a wide plethora of flexible electrochemical sensors.

2.3. Electrocatalytic Determination of NADH

The NAD^+/NADH system is the co-factor for many dehydrogenase-type enzymes; for this reason, it constitutes the actual electroactive species finally detected by enzymatic biosensors developed for the quantification of various analytes. According to previous works concerning the use of GRM for the electrochemical detection of NADH,[21,26] oxidized moieties present on carbon nanosheets allow the activation of effective electrocatalytic processes causing NADH oxidation, highly increasing the sensitivity of the sensor response with respect to graphite-based electrodes; as obtained from XPS results (see Table S2 in the Supporting Information). These moieties are also present on the surface of GPP. **Figure 5**a reports the voltammetric response recorded at GPP for 1.0×10^{-3} M NADH oxidation, in comparison to responses obtained in the same solution at C-SPE and Gr-SPE (original CV traces in the absence and in the presence of the analyte are reported in Figure S12 in the Supporting Information). This highlights that G-paper is effective in inducing electrocatalytic oxidation of NADH without any pretreatment of the surface; oxidation of this species starts occurring at ≈+0.1 V at GPP, i.e., 0.30 and 0.35 V before than

that obtained at C-SPE and Gr-SPE, respectively. A well-defined oxidation peak, previously ascribed to electroactive alcoholic residues present on the surface,[21,26] is observed at ≈+0.25 V. Similar electrocatalytic activity was also observed after coating commercial electrochemical platforms with GRM films;[21] however, functionalization of commercial conductive platforms complicates the production of effective sensors and reduces, at the same time, the reproducibility of the response. As already stated, the presence of well-resolved oxidation peak at ≈+0.25 V is maintained even after peeling the outermost few layers of the GPP surface (Figure S13, Supporting Information), indicating that the evident electrocatalytic process observed is ascribable to the very low number of oxidized functional groups present on G-paper and not to oxidized Si moieties present on the surface (see XPS analysis). On the other hand, any attempt to compare, in more detail, the performance of the three-electrode platforms considered on the basis of the surface functional groups is not possible, since the presence of C—Cl residues in commercial devices completely hinders the contribution of oxidized carbon residues in the C 1s spectra. Similar electrocatalytic properties are retained even changing the underlying electrode support, since GPP built both on textile and on Kapton showed a similar response (see Figure S14 in the Supporting Information).

The possible application of GPPs as reliable sensors for NADH, i.e., for the realization of biosensors, was also testified by the very good repeatability of consecutive voltammetric responses recorded on the same GPP, showing an RSD of 5.4% calculated for the value of peak current at +0.25 V (Figure S15, Supporting Information). This demonstrates that fouling effects, commonly affecting the voltammetric response of this analyte,[65–67] are almost absent on GPP.

The analytical performance of GPP for NADH detection was once more studied by FIA; the working electrode was polarized at +0.35 V, obtaining the response reported in Figure 5b. The relevant calibration plot (inset of Figure 5b) shows a good
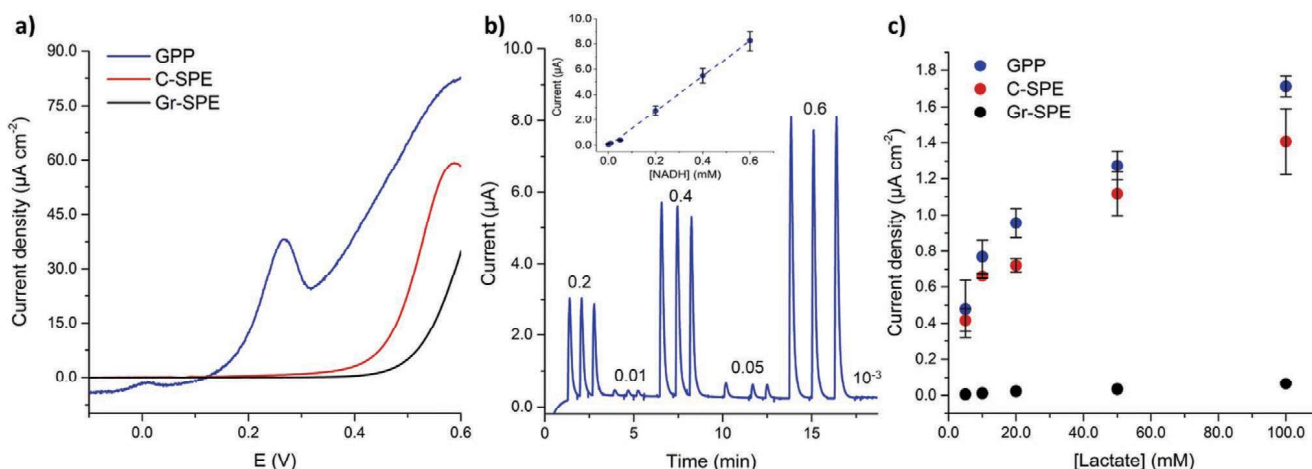
Figure 5. a) CV responses of 1×10^{-3} M NADH in 0.1 M PBS and 0.1 M KCl recorded at GPP on PET, C-SPE, and Gr-SPE; each curve shows the forward voltammetric scan after subtraction of the relevant blank signal (full curves with the original data are reported in Figure S9 in the Supporting Information). b) FIA response for NADH detection obtained at GPP by polarizing the working electrode at the fixed potential of +0.35 V and by injecting NADH at concentration levels ranging from 1×10^{-6} to 0.6×10^{-3} M; the concentration (in $\times 10^{-3}$ M) of NADH in the solutions injected is reported in correspondence of the relevant signals obtained; the inset reports the relevant calibration plot obtained at three different GPPs with standard deviation calculated at each point from at least three replicates of each solution. c) Calibration curves obtained in FIA for ʟ-lactate at +0.50 V on GPP, and at +0.70 V on C-SPE and on Gr-SPE; relevant standard deviation is reported for each concentration level calculated from three injections of the same solution.

Table 1. Analytical performance of GPP for NADH detection in amperometric detection compared to different electrode systems described in literature (GC: glassy carbon electrode; rGO: reduced graphene oxide; EGO: electrochemically exfoliated graphene oxide; PMB: poly(methylene blue); NPs: nanoparticles; APBA: 3-aminophenilboronic acid; PMS: phenazine methosulfate; MWCNT: multiwalled carbon nanotubes; PAH: poly(allylamine hydrochloride); AB: azure B; PB: Prussian blue; Gr: graphite electrode; SWCNT-Os: single-walled carbon nanotubes mixed to poly(vinylpyridine) [osmium-(N,N-methylated-[2,2]-biimidalzole)$_3$]$^{2+/3+}$; DI: diaphorase; PEGDGE: poly(ethylene glycol) diglycidyl ether; SWCNTE: single-walled carbon nanotube electrode; CFA: caffeic acid; CA: chronoamperometry).

Sensing system	Detection technique	Sensitivity [$\mu A\ m_M^{-1}\ cm^{-2}$]	LOD [$\times 10^{-6}$ M]	Linear range [$\times 10^{-3}$ M]	Potential vs Ag/AgCl [V]	Ref.
Functionalized with pristine nanomaterials						
GC/rGO	CA	39.41	10.0	0.04–0.8	+0.45	[68]
GC/C-nanofibers	CA	3.64	11.0	0.03–2.14	+0.35	[69]
C-SPE/EGO	CA	73.3	–	0.002–0.027	+0.20	[21]
Functionalized with nanomaterials and organic moieties						
C-SPE/carbon black/caffeic acid	CA	169.9	1.6	0.001–0.8	+0.25	[70]
GC/AuNPs/rGO-chitosan	CA	318	1.2	0.002–0.320	+0.35	[71]
G-paper/PMB/AgNPs	CA	161	0.07	0.00025–0.4	+0.54	[55]
GC/APBA-MWCNT/PMS	CA	161	0.2	0.0005–1	−0.10	[72]
C-SPE/rGO–PAH	CA	108.6	6.0	0.04–0.8	+0.45	[73]
Au(111)/AB–EGO	CA	510	0.15	0.0005–0.5	+0.78	[74]
Gr-SPE/PB/PMS	CA	336	0.5	0.001–0.1	−0.05	[75]
Gr/SWCNT-Os/DI/PEGDGE	FIA	47	0.05	0.005–7.0	−0.18	[76]
SWCNTE/CFA	CA	70.8	–	0.002–0.030	+0.30	[77]
Nonfunctionalized						
GPP	FIA	107.2	0.6	0.001–0.6	+0.35	This work

linear correlation ($R^2 = 0.99$) between the current peak and the concentration of analyte, as well as a high repeatability of the sensor response (RSD = 3.4%, calculated for eight injections at 0.2×10^{-3} M). As already observed for Fc oxidation, the baseline of the amperometric response is highly stable despite the values of background currents characterizing GPPs, once more demonstrating the electrochemical stability of GPPs. This property has once more beneficial effect in the quite low limit of detection found (0.6×10^{-6} M), since it is calculated from the standard deviation of the signal in the absence of analyte.

We compared the analytical performance for NADH sensing on GPP with other nonenzymatic electrochemical sensors, only considering sensing elements that can be used in flexible devices and contain, or are entirely made of, carbon nanosized materials, eventually including organic moieties to further improve the sensitivity of the response (**Table 1**). As observed, to the best of our knowledge, GPP is the first example of flexible electrochemical platform used as such, i.e., without any further modification of the electrode surface, to detect NADH. Moreover, it can give very high sensitivity, low LOD, and a good linear range, much better than electrodes based on nanomaterials; the sensitivity and LOD are comparable to what obtained instead with electrodes functionalized with additional steps, i.e., adding organic moieties. GPPs have a clear advantage on such electrodes because they do not require additional functionalization steps.

The excellent sensitivity recorded at GPP is obtained despite the application of a low potential value, namely +0.35 V; similar results can be achieved at graphite-based electrodes only after modification of the surface. Sensitivity data for bare electrodes

are not present in the literature, and we did not perform tests either with C-SPE or with Gr-SPEs in this work since the calibration plot should have been performed at higher potential values to be comparable, as well evident from responses reported in Figure 5a. In conclusion, despite the simplicity in the manufacturing of the device, GPP features a high sensitivity for NADH detection, superior to all the other electrodes functionalized by nanomaterials, and only comparable to that of more complex electrochemical systems, fabricated via multilayer processing or including organic moieties.

2.4. Tests for the Applicability of GPP as a Biosensor

The versatility of the use of GPPs was proven by testing their behavior as biosensors; as a proof of concept for the applicability of this electrode platform in this field, we anchored an enzyme requiring the NAD$^+$/NADH redox system as the cofactor (namely LDH) on the electrode surface using a diazonium salt bearing a carboxylic functional group.[78] LDH allows the detection of lactate through the following enzymatic reaction

$$L-lactate + NAD^+ \xrightarrow{LDH} Pyruvate + NADH + H^+ \tag{1}$$
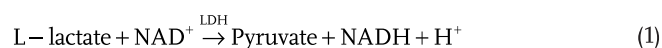
According to this reaction, the amount of lactate present in the solution can be determined by the oxidation responses of NADH produced by the enzymatic reaction. As already outlined, the possibility of oxidizing this electroactive species at less positive potentials with respect to pristine carbon-based

electrodes would increase the selectivity of the developed sensor. To study the possibility of employing GPPs for enzymatic lactate detection, FIAs were performed by polarizing the working electrode at +0.50 V. These tests were also repeated on C-SPE and Gr-SPE functionalized in the same way; however, as stated before, these measurements were recorded by polarizing the electrode at a higher potential value, namely +0.70 V, due to the absence of electrocatalytic effects toward NADH oxidation at these electrode surfaces (Figure 5a). The obtained calibration plot (Figure 5c) highlights the possibility of employing GPPs for lactate detection at lower potential values with respect to other commercial carbon-based electrodes. These preliminary results confirm the possibility of detecting NADH also on the GPP functionalized with an enzyme and open to the possibility of using this device in enzymatic biosensing.

3. Conclusions

In this work, we developed a new, robust, flexible, three-electrode device made of G-paper, showing its advantages with respect to bare carbon-based commercial SPEs. The GPPs, supported on plastic or on cotton, were successfully employed in electrochemical tests, confirming the possibility of using these devices as electrodes, also for on-line detection systems.

Exploiting the properties of graphene, mainly ascribable to surface functional groups and to the 2D morphology, electrocatalysis of NADH is achieved with remarkable analytical performance directly on the bare device, without the need for further functionalization of the surface, thus avoiding the drawbacks of a coating; this results in an electrochemical sensor for NADH detection possessing a sensitivity of 107.2 μA m$_M^{-1}$ cm^{-2} and a limit of detection of 0.6×10^{-6} M. The preliminary on-line tests performed after the anchoring of lactate dehydrogenase showed that the electrocatalytic properties of G-paper are maintained also in the final configuration, i.e., for NADH molecules enzymatically produced, demonstrating that this material can be a robust and versatile substrate for a wide range of sensing applications.

As a further advantage in the use of G-paper-based platform, the mesoporous structure of the material may allow the inclusion of additional components, e.g., redox active species or nanomaterials, to obtain effective electrochemical platforms for the detection of different species, e.g., the hydrogen peroxide produced from oxidase-type enzymes.

Since G-paper can be easily processed on rigid or flexible substrates, including plastic, textiles, and clothing, the brand-new biosensing application demonstrated in this work opens new possibilities for comprehensive wearable electronic devices. The advantages also include the price of G-paper. For large-scale production the target price is around 250 euro m^{-2} that means a few cents euro of material per electrode and the possibility of recycling the waste of material eliminated by the cutting approach for the production of new G-paper.

4. Experimental Section

Preparation of GPPs: G-paper (G2nan-sheet GS50), prepared from graphite nanoplatelets, was purchased by Nanesa (Italy).

GPPs were made using different strategies, as reported in Figure 1. Devices on cotton and PET were prepared by the cutting process (strategy A). G-paper was patterned with the desired shape by a robotic cutting plotter from Silhouette Cameo (blade level = 100 μm, grammage = 28 g m^{-2}, and speed = 10 cm s^{-1}) or a laser system Trotec Speedy 100 Flexx (pulsed fiber laser; cutting settings: power = 100%, speed = 10%, frequency = 20 kHz, and passes = 4). The negative part of the shape was removed, and the electrodes obtained were attached to a PET foil coated with a thermoplastic glue (laminating pouch film SIAM, thickness = 250 μm) or on cotton textile (cotton cloth Bellora, thickness = 170 μm) coated with thermoplastic polyurethane (Delstar International—EU29). The coupling between G-paper and the substrate was performed by hot lamination or by a hot press. GPPs on polyimide substrates were prepared by the laser ablation process (strategy B). G-paper was first attached to a Kapton tape (5 mil polyimide tape silicone adhesive from Caplinq) and then the GPPs were obtained by ablation of the negative part of graphene by laser (pulsed fiber laser; engraving settings: power = 60%, speed = 50%, frequency = 60 kHz, and passes = 10). The optimized manufacture of GPPs on several supports allowed them to be possibly exploited for on-skin or on-clothes (bio)sensing and even for electrochemical applications at extreme temperature conditions.

GPPs were used for electrochemical applications without any pretreatment. The geometric area of the working electrode, 0.126 cm^2, was set by covering the conductive tracks with an insulating paint. The reference electrode was coated with Ag^0 paste; to obtain a stable and reproducible potential, 0.1 M KCl was added to all the solutions used for electrochemical tests. Proofs of the potential shift when the Ag reference electrode was not employed are shown in Figure S16 (Supporting Information).

For L-lactate detection, the enzyme LDH (from Roche) was anchored on the working electrode of GPP through 4-carboxyphenyldiazonium (tetrafluoroborate) (Ph—COOH). This salt was synthesized according to a procedure previously reported,[79] and functionalization of the electrode surface was achieved by an electrochemical approach.[80] The potential was linearly varied from +0.4 to −0.80 at 0.1 V s^{-1}, after dropping on the three-electrode platform for a solution of 2×10^{-3} M Ph—COOH in 0.1 M H$_2$SO$_4$. Activation of the carboxylic functional groups occurred by depositing on the working electrode a 5×10^{-3} M solution of *N*-(3-dimethylaminopropyl)-*N'*-ethylcarbodiimide hydrochloride (EDC) in 0.1 M 2-(*N*-morpholino)ethanesulfonic acid (MES) buffer (pH 6.0) for 10 min, followed by the addition of an equal volume of a 5×10^{-3} M solution of *N*-hydroxysuccinimide (NHS) in 0.1 M MES (pH 6.0). After further 10 min, the surface was abundantly washed with ultrapure water, and 15.0 μL of 550 U mg^{-1} (5 g L^{-1}) LDH solution was deposited and left drying at +4 °C overnight. Finally, 2.5 μL of 1% Nafion solution (Merck-Sigma Aldrich), neutralized with NaOH, was added to obtain a more stable anchoring of the enzyme.

Instrumentation: XPS responses were acquired by a Phoibos 100 hemispherical energy analyzer (Specs, Germany) using Mg Kα radiation ($\hbar\omega$ = 1253.6 eV). The X-ray power was set to 125 W. The spectra were recorded in the constant analyzer energy (CAE) mode with analyzer pass energies of 10 eV for the high-resolution spectra. The base pressure in the analysis chamber during analysis was 1×10^{-8} mbar. GPP was analyzed as such and after peeling the surface by a Magic Tape (3M, USA), constituting a procedure often used to obtain fresh surfaces in layered material (i.e., in highly oriented pyrolytic graphite). High-resolution XPS spectra of C 1s were analyzed by CasaXPS (Casa Software, Ltd.); the curve fitting was carried out using Gaussian/Lorentzian curves shape (GL(30)) for C—O groups with a full width half-maximum of 1.4 eV and an asymmetric Voigt for the C—C sp^2.

SEM images of GPP were recorded by using LEO 1530 FEG (ZEISS, Germany), operating at 5 kV; secondary electrons were collected by means of an In-Lens detector.

All the electrochemical measurements were performed with an Autolab PGSTAT12 potentiostat/galvanostat (Metrohm) and a μStat 400 portable bi-potentiostat/galvanostat (Metrohm-DropSens). Electrical connection of GPPs to potentiostat was obtained by inserting

the electrode in a cable connector for commercial SPEs (Metrohm-Dropsens). C-SPEs were acquired from Metrohm-Dropsens (model 110); they consisted of a 0.13 cm^2 carbon working electrode, a carbon auxiliary electrode, and a Ag pseudoreference electrode. Gr-SPEs were acquired from Sense4Med (Rome, Italy); they consisted of a 0.07 cm^2 graphite working electrode, a graphite auxiliary electrode, and a Ag pseudoreference electrode.

Electrochemical analyses were performed at room temperature and in equilibrium with the atmosphere, i.e., in the presence of O_2. The first set of measurements, aimed at defining the performance of GPP in electrochemical measurements, was recorded by simply adding a drop of solution (≈60 µL) on the surface of the three-electrode cell. In another set of measurements, GPP was placed in an instrumental configuration typical of FIA. The electrode was inserted in a flow cell (Metrohm-Dropsens), aiming at defining the analytical performance of the device. The flow of electrolyte was kept constant at 1.0 mL min^{-1} using a Minipuls 3 (Gilson) peristaltic pump while injecting the electroactive species in the electrochemical cell through a Rheodyne valve possessing a volume of 100 µL.

For EIS measurements, external counter and reference electrodes, namely a Pt wire and Ag/AgCl/3 M KCl (Amel), were inserted at fixed position to complete the electrochemical cell with the working electrodes of either GPP, C-SPE, or Gr-SPE. These measurements were performed with an Autolab PGSTAT30 potentiostat/galvanostat (Metrohm)

Sheet resistance of GPP, C-SPE, or Gr-SPE working electrodes was measured in 4-point probe van der Pauw configuration; contacts were obtained by using silver conductive paste, and *IV* curves were measured in the range of ±100 mA for GPP and ±1 mA for C-SPE and Gr-SPE.

BET surface area was measured by ASAP 2020 (Micromeritics).

Electrochemical Tests: All solutions for electrochemical tests were obtained in deionized water possessing a resistivity of 18 MΩ cm. The possible application of GPP as an electrochemical platform was tested by CV in 0.1 M LiClO$_4$ solutions, in the absence and presence of 0.5×10^{-3} M Fc (Merck-Sigma Aldrich). Subsequent voltammetric scans between −0.10 and +0.60 V were recorded at a 0.05 V s^{-1} potential scan rate. The same solution was also used to test the application of GPP in DPV; in this case, the pulse amplitude was set at 50 mV, the step potential at 6 mV, the pulse time at 0.1 s, and the scan rate was 15 mV s^{-1}.

EIS measurements were recorded in a 5×10^{-3} M K$_4$Fe(CN)$_6$, 5×10^{-3} M K$_3$Fe(CN)$_6$, 0.1 M KCl solution, by applying an AC voltage with 5 mV perturbation (0.05–10 000 Hz frequency range) at open-circuit potential. The Nyquist plots obtained were fitted to calculate the charge-transfer resistance.

Further tests were performed in 0.1 M phosphate-buffered saline (PBS) solution at pH 7.00, recording voltammetric scans between −0.60 V and +0.60 V, at a 0.02 V s^{-1} potential scan rate. The response of the sensor for NADH (Merck-Sigma Aldrich) oxidation was recorded by dissolving this species in 0.1 M PBS and by recording CV experiments in the −0.10 ÷ (+0.60) V potential interval, at a 0.02 V s^{-1} potential scan rate. The response for each CV experiment was reported after reaching the steady state, except when differently indicated.

The analytical performance of GPPs for NADH and L-lactate (Merck-Sigma Aldrich) detection was defined mimicking an on-line measuring system by FIA, after checking the electrochemical behavior of GPP in this configuration with a reversible redox probe, namely Fc. For these measurements, the working electrode was polarized at a constant potential of +0.30 V, and 100 µL of solutions containing the analyte was injected inside the flow of the pure electrolyte solution. Solutions at different concentration levels were analyzed randomly to avoid the possible occurrence of memory effects. 5×10^{-3} M NAD$^+$ (Merck-Sigma Aldrich) co-factor was also added to all the solutions employed for L-lactate detection, prepared in PBS.

For the sake of comparison, similar measurements were also repeated on C-SPEs and on Gr-SPEs; the volumes used for these tests were calculated according to the different geometric areas of these electrodes to achieve similar volume/surface ratio.

Supporting Information

Supporting Information is available from the Wiley Online Library or from the author.

Acknowledgements

Conflict of Interest

The authors declare no conflict of interest.

Data Availability Statement

The data that support the findings of this study are available from the corresponding author upon reasonable request.

Keywords

[1] N. Komuro, S. Takaki, K. Suzuki, D. Citterio, *Anal. Bioanal. Chem.* **2013**, *405*, 5785.
[2] J. Kim, R. Kumar, A. J. Bandodkar, J. Wang, *Adv. Electron. Mater.* **2017**, *3*, 1600260.
[3] V. Katseli, A. Economou, C. Kokkinos, *Electrochem. Commun.* **2019**, *103*, 100.
[4] N. Batra, M. Tomar, P. Jain, V. Gupta, *J. Appl. Phys.* **2013**, *114*, 124702.
[5] A. S. Afonso, C. V. Uliana, D. H. Martucci, R. C. Faria, *Talanta* **2016**, *146*, 381.
[6] J. Li, F. Rossignol, J. Macdonald, *Lab Chip* **2015**, *15*, 2538.
[7] D. Sharp, R. Burkitt, *Mater. Technol.* **2015**, *30*, B155.
[8] R. Seeber, F. Terzi, C. Zanardi, *Functional Materials in Amperometric Sensing*, Springer, Berlin **2014**.
[9] R. Seeber, L. Pigani, F. Terzi, C. Zanardi, *Electrochim. Acta* **2015**, *179*, 350.
[10] P. Pinyou, V. Blay, L. M. Muresan, T. Noguer, *Mater. Horiz.* **2019**, *6*, 1336.
[11] N. Thiyagarajan, J. L. Chang, K. Senthilkumar, J. M. Zen, *Electrochem. Commun.* **2014**, *38*, 86.
[12] P. L. dos Santos, V. Katic, H. C. Loureiro, M. F. dos Santos, D. P. dos Santos, A. L. B. Formiga, J. A. Bonacin, *Sens. Actuators, B* **2019**, *281*, 837.
[13] T. A. Enache, A. Amine, C. M. A. Brett, A. M. Oliveira-Brett, *Talanta* **2013**, *105*, 179.
[14] K. Charoenkitamorn, S. Chaiyo, O. Chailapakul, W. Siangproh, *Anal. Chim. Acta* **2018**, *1004*, 22.

[15] F. Ricci, A. Amine, C. S. Tuta, A. A. Ciucu, F. Lucarelli, G. Palleschi, D. Moscone, *Anal. Chim. Acta* **2003**, *485*, 111.

[16] S. Liu, T. Wu, F. Li, Q. Zhang, X. Dong, L. Niu, *Anal. Methods* **2018**, *10*, 1986.

[17] F. Arduini, F. Di Nardo, A. Amine, L. Micheli, G. Palleschi, D. Moscone, *Electroanalysis* **2012**, *24*, 743.

[18] C. Backes, A. M. Abdelkader, C. Alonso, A. Andrieux-Ledier, R. Arenal, J. Azpeitia, N. Balakrishnan, L. Banszerus, J. Barjon, R. Bartali, S. Bellani, C. Berger, R. Berger, M. M. B. Ortega, C. Bernard, P. H. Beton, A. Beyer, A. Bianco, P. Bøggild, F. Bonaccorso, G. B. Barin, C. Botas, R. A. Bueno, D. Carriazo, A. Castellanos-Gomez, M. Christian, A. Ciesielski, T. Ciuk, M. T. Cole, J. Coleman, et al., *2D Mater.* **2020**, *7*, 022001.

[19] Y. Zhong, Z. Zhen, H. Zhu, *FlatChem* **2017**, *4*, 20.

[20] A. Bonanni, A. Ambrosi, C. K. Chua, M. Pumera, *ACS Nano* **2014**, *8*, 4197.

[21] G. Maccaferri, C. Zanardi, Z. Y. Xia, A. Kovtun, A. Liscio, F. Terzi, V. Palermo, R. Seeber, *Carbon* **2017**, *120*, 165.

[22] A. Ambrosi, M. Pumera, *Chem. - Eur. J.* **2013**, *19*, 4748.

[23] K. P. Prathish, M. M. Barsan, D. Geng, X. Sun, C. M. A. Brett, *Electrochim. Acta* **2013**, *114*, 533.

[24] F. Poletti, L. Favaretto, A. Kovtun, E. Treossi, F. Corticelli, M. Gazzano, V. Palermo, C. Zanardi, M. Melucci, *J. Phys. Mater.* **2020**, *3*, 014011.

[25] G. H. Yang, D. D. Bao, H. Liu, D. qing Zhang, N. Wang, H. tao Li, *J. Inorg. Organomet. Polym. Mater.* **2017**, *27*, 1129.

[26] F. Vulcano, A. Kovtun, C. Bettini, Z. Xia, A. Liscio, F. Terzi, A. Heras, A. Colina, B. Zanfrognini, M. Melucci, V. Palermo, C. Zanardi, *2D Mater.* **2020**, *7*, 024007.

[27] J. Mohanraj, D. Durgalakshmi, R. Ajay Rakkesh, *J. Electrochem. Soc.* **2020**, *167*, 067523.

[28] E. Jabari, F. Ahmed, F. Liravi, E. B. Secor, L. Lin, E. Toyserkani, *2D Mater.* **2019**, *6*, 042004.

[29] A. Bonanni, A. Ambrosi, M. Pumera, *Chem. - Eur. J.* **2012**, *18*, 4541.

[30] A. Ambrosi, C. K. Chua, A. Bonanni, M. Pumera, *Chem. Rev.* **2014**, *114*, 7150.

[31] M. Zhang, C. Hou, A. Halder, H. Wang, Q. Chi, *Mater. Chem. Front.* **2017**, *1*, 37.

[32] M. Zhang, A. Halder, C. Hou, J. Ulstrup, Q. Chi, *Bioelectrochemistry* **2016**, *109*, 87.

[33] C. Teng, D. Xie, J. Wang, Z. Yang, G. Ren, Y. Zhu, *Adv. Funct. Mater.* **2017**, *27*, 1700240.

[34] A. Scidà, S. Haque, E. Treossi, A. Robinson, S. Smerzi, S. Ravesi, S. Borini, V. Palermo, *Mater. Today* **2018**, *21*, 223.

[35] R. Karthick, F. Chen, *Carbon* **2019**, *150*, 292.

[36] T. Hu, X. Sun, H. Sun, M. Yu, F. Lu, C. Liu, J. Lian, *Carbon* **2013**, *51*, 322.

[37] R. Wang, C. Xu, J. Sun, Y. Liu, L. Gao, C. Lin, *Nanoscale* **2013**, *5*, 6960.

[38] A. Yu, A. Sy, A. Davies, *Synth. Met.* **2011**, *161*, 2049.

[39] D. Pullini, V. Siong, D. Tamvakos, B. Lobato Ortega, M. F. Sgroi, A. Veca, C. Glanz, I. Kolaric, A. Pruna, *Compos. Sci. Technol.* **2015**, *112*, 16.

[40] A. Singh, A. J. Roberts, R. C. T. Slade, A. Chandra, *J. Mater. Chem. A* **2014**, *2*, 16723.

[41] D. A. L. Almeida, A. B. Couto, N. G. Ferreira, *J. Alloys Compd.* **2019**, *788*, 453.

[42] H. Choi, K.-J. Ahn, Y. Lee, S. Noh, H. Yoon, *Adv. Mater. Interfaces* **2015**, *2*, 1500117.

[43] D. Xu, Q. Xu, K. Wang, J. Chen, Z. Chen, *ACS Appl. Mater. Interfaces* **2014**, *6*, 200.

[44] X. Yan, J. Chen, J. Yang, Q. Xue, P. Miele, *ACS Appl. Mater. Interfaces* **2010**, *2*, 2521.

[45] M. Lee, B.-H. Wee, J.-D. Hong, *Adv. Energy Mater.* **2015**, *5*, 1401890.

[46] Y.-C. Hsu, L.-C. Tseng, R.-H. Lee, *J. Polym. Sci., Part B: Polym. Phys.* **2014**, *52*, 321.

[47] M. J. Ju, I.-Y. Jeon, J. C. Kim, K. Lim, H.-J. Choi, S.-M. Jung, I. T. Choi, Y. K. Eom, Y. J. Kwon, J. Ko, J.-J. Lee, H. K. Kim, J.-B. Baek, *Adv. Mater.* **2014**, *26*, 3055.

[48] J. Gong, Z. Zhou, K. Sumathy, H. Yang, Q. Qiao, *J. Appl. Phys.* **2016**, *119*, 135501.

[49] D. Pierleoni, Z. Y. Xia, M. Christian, S. Ligi, M. Minelli, V. Morandi, F. Doghieri, V. Palermo, *Carbon* **2016**, *96*, 503.

[50] H. Liu, T. Kuila, N. H. Kim, B. C. Ku, J. H. Lee, *J. Mater. Chem. A* **2013**, *1*, 3739.

[51] J. T. Chen, Y. J. Fu, Q. F. An, S. C. Lo, S. H. Huang, W. S. Hung, C. C. Hu, K. R. Lee, J. Y. Lai, *Nanoscale* **2013**, *5*, 9081.

[52] N. Zhu, S. Han, S. Gan, J. Ulstrup, Q. Chi, *Adv. Funct. Mater.* **2013**, *23*, 5297.

[53] R.-M. Song, Z.-H. Li, P.-J. Wei, X.-L. Zhao, C. Chen, Z.-G. Zhu, *Appl. Sci.* **2018**, *8*, 848.

[54] S. Dong, J. Xi, Y. Wu, H. Liu, C. Fu, H. Liu, F. Xiao, *Anal. Chim. Acta* **2015**, *853*, 200.

[55] E. Topçu, K. Dağcı, M. Alanyalıoğlu, *Electroanalysis* **2016**, *28*, 2058.

[56] V. Kumar, I. Kaur, S. Arora, R. Mehla, K. Vellingiri, K. H. Kim, *Food Chem.* **2020**, *303*, 125375.

[57] R. K. Srivastava, S. Srivastava, T. N. Narayanan, B. D. Mahlotra, R. Vajtai, P. M. Ajayan, A. Srivastava, *ACS Nano* **2012**, *6*, 168.

[58] C. S. Lim, C. K. Chua, M. Pumera, *Analyst* **2014**, *139*, 1072.

[59] J. P. Metters, R. O. Kadara, C. E. Banks, *Analyst* **2011**, *136*, 1067.

[60] B. Schnyder, T. Lippert, R. Kötz, A. Wokaun, V. M. Graubner, O. Nuyken, *Surf. Sci.* **2003**, *532*, 1067.

[61] A. Kovtun, D. Jones, S. Dell'Elce, E. Treossi, A. Liscio, V. Palermo, *Carbon* **2019**, *143*, 268.

[62] S. Yang, S. Brüller, Z. S. Wu, Z. Liu, K. Parvez, R. Dong, F. Richard, P. Samorì, X. Feng, K. Müllen, *J. Am. Chem. Soc.* **2015**, *137*, 13927.

[63] S. Sibilia, F. Bertocchi, S. Chiodini, F. Cristiano, L. Ferrigno, G. Giovinco, A. Maffucci, *Nanotechnology* **2021**, *32*, 275701.

[64] F. Poletti, B. Zanfrognini, L. Favaretto, V. Quintano, J. Sun, E. Treossi, M. Melucci, V. Palermo, C. Zanardi, *Sens. Actuators, B* **2021**, *344*, 130253.

[65] S. Immanuel, R. Sivasubramanian, *Mater. Chem. Phys.* **2020**, *249*, 123015.

[66] L. Blandón-Naranjo, J. Hoyos-Arbeláez, M. V. Vázquez, F. Della Pelle, D. Compagnone, *J. Sensors* **2018**, *2018*, 6525919.

[67] S. A. Kumar, S.-M. Chen, *Sensors* **2008**, *8*, 739.

[68] M. Zhou, Y. Zhai, S. Dong, *Anal. Chem.* **2009**, *81*, 5603.

[69] A. Arvinte, F. Valentini, A. Radoi, F. Arduini, E. Tamburri, L. Rotariu, G. Palleschi, C. Bala, *Electroanalysis* **2007**, *19*, 1455.

[70] C. Zanardi, E. Ferrari, L. Pigani, F. Arduini, R. Seeber, *Chemosensors* **2015**, *3*, 118.

[71] H. Chang, X. Wu, C. Wu, Y. Chen, H. Jiang, X. Wang, *Analyst* **2011**, *136*, 2735.

[72] J. Li, Q. Sun, Y. Mao, Z. Bai, X. Ning, J. Zheng, *J. Electroanal. Chem.* **2017**, *794*, 1.

[73] O. M. Istrate, L. Rotariu, C. Bala, *Microchim. Acta* **2016**, *183*, 57.

[74] O. Bayindir, M. Alanyalioglu, *IEEE Sens. J.* **2019**, *19*, 812.

[75] F. Ricci, A. Amine, D. Moscone, G. Palleschi, *Biosens. Bioelectron.* **2007**, *22*, 854.

[76] C. Deng, J. Chen, X. Chen, C. Xiao, Z. Nie, S. Yao, *Electrochem. Commun.* **2008**, *10*, 907.

[77] A. Heras, F. Vulcano, J. Garoz-Ruiz, F. Porcelli, F. Terzi, A. Colina, R. Seeber, C. Zanardi, *Sensors* **2019**, *19*, 518.

[78] D. Hetemi, V. Noël, J. Pinson, *Biosensors* **2020**, *10*, 4.

[79] C. Saby, B. Ortiz, G. Y. Champagne, D. Bélanger, *Langmuir* **1997**, *13*, 6805.

[80] K. M. Herdman, C. B. Breslin, N. J. Finnerty, *J. Electroanal. Chem.* **2018**, *828*, 137.